arXiv:1511.06784v2 [hep-ph] 2 Feb 2016

Double parton scattering: Impact of nonperturbative parton correlations

Sergey Ostapchenko[1,2] and Marcus Bleicher[1,3]

[1] *Frankfurt Institute for Advanced Studies, 60438 Frankfurt am Main, Germany*

[2] *D.V. Skobeltsyn Institute of Nuclear Physics, Moscow State University, 119992 Moscow, Russia*

[3] *Institute for Theoretical Physics, Goethe-Universitat, 60438 Frankfurt am Main, Germany*

February 3, 2016

Abstract

We apply the phenomenological Reggeon field theory framework to investigate the relative importance of perturbative and nonperturbative multiparton correlations for the treatment of double parton scattering (DPS) in proton-proton collisions. We obtain a significant correction to the so-called effective cross section for DPS due to nonperturbative parton splitting. When combined with the corresponding perturbative contribution, this results in a rather weak energy and transverse momentum dependence of the effective cross section, in agreement with experimental observations at the Tevatron and the Large Hadron Collider. In addition, we observe that color fluctuations have a sizable impact on the calculated rate of double parton scattering and on the relative importance of the perturbative parton splitting mechanism.

1 Introduction

There is currently considerable interest, both from the theoretical and the experimental sides, to study multiparton interactions. Apart from being an efficient tool for probing the spatial distribution of partons in hadrons, such processes constitute a major background for searches of new physics. Consequently, the treatment of multiparton interactions is an important ingredient of contemporary Monte Carlo generators of hadronic collisions, both at the energies of the LHC and at yet higher cosmic ray energies.

Indirect evidence for multiple inelastic parton scatterings comes from a comparison of calculated inclusive cross sections for (mini)jet production in proton-proton collisions with the total inelastic pp cross section $\sigma_{pp}^{\rm inel}$: for sufficiently small jet transverse momenta, the inclusive jet cross section substantially exceeds $\sigma_{pp}^{\rm inel}$ in the very high energy limit. This means that a number of jet production processes should take place simultaneously. Direct evidence for double parton interactions has been obtained experimentally, both at the Tevatron and LHC [1, 2, 3, 4].

The pioneering theoretical works on multiparton interactions (MPIs) date 30 years back [5, 6, 7], together with the first attempts to implement them in Monte Carlo generators [8]. Recently, considerable progress has been achieved in understanding the MPI physics and developing the theory for multiparton interactions [9, 10, 11, 12, 13, 14, 15, 16].

The relative rate of double parton scattering (DPS) may be quantified by the so-called effective cross section defined (here, for the case of two hadronic dijets production in proton-proton collisions) as

$$\sigma_{pp}^{\rm eff}(s,p_{\rm t}^{\rm cut}) = \frac{1}{2}\,\frac{\left[\sigma_{pp}^{\rm 2jet}(s,p_{\rm t}^{\rm cut})\right]^2}{\sigma_{pp}^{\rm 4jet(DPS)}(s,p_{\rm t}^{\rm cut})}\,, \qquad (1)$$

where $\sigma_{pp}^{\rm 2jet}(s,p_{\rm t}^{\rm cut})$ is the inclusive cross section for the production of a pair of jets of transverse momentum $p_{\rm t} > p_{\rm t}^{\rm cut}$, $\sigma_{pp}^{\rm 4jet(DPS)}(s,p_{\rm t}^{\rm cut})$ is the cross section for DPS production of two dijets of $p_{\rm t} > p_{\rm t}^{\rm cut}$, $(1/2)$ is a symmetry factor, and s is the center-of-mass energy squared.

The inclusive jet cross section is defined by the usual collinear factorization ansatz

$$\sigma_{pp}^{\rm 2jet}(s,p_{\rm t}^{\rm cut}) = \int dx^+dx^- \int_{p_{\rm t}>p_{\rm t}^{\rm cut}} dp_{\rm t}^2$$

$$\times \sum_{I,J=q,\bar{q},g} f_I(x^+, M_{\rm F}^2)\, f_J(x^-, M_{\rm F}^2)\, \frac{d\sigma_{IJ}^{2\to 2}}{dp_{\rm t}^2}\,, \quad (2)$$

with $x^\pm$ being the light-cone momentum fractions, $d\sigma_{IJ}^{2\to 2}/dp_{\rm t}^2$ the parton scatter cross section, and $f_I(x, M_{\rm F}^2)$ the parton I momentum distribution function (PDF) evaluated at the factorization scale $M_{\rm F}^2$.

In turn, $\sigma_{pp}^{\rm 4jet(DPS)}$ involves the so-called generalized two-parton distribution ($_2$GPD) $F^{(2)}_{I_1I_2}(x_1, x_2, q_1^2, q_2^2, \Delta\!\!\!/b)$ which describes the momentum distribution of a pair of partons probed at the virtuality scales q_1^2 and q_2^2, separated by the transverse distance $\Delta\!\!\!/b$ [9, 10, 14]:[1]

$$\sigma_{pp}^{\rm 4jet(DPS)}(s, p_{\rm t}^{\rm cut}) = \frac{1}{2}\int dx_1^+ dx_2^+ dx_1^- dx_2^-$$
$$\times \int_{p_{\rm t_1}, p_{\rm t_2} > p_{\rm t}^{\rm cut}} dp_{\rm t_1}^2\, dp_{\rm t_2}^2 \sum_{I_1,I_2,J_1,J_2} \frac{d\sigma_{I_1J_1}^{2\to 2}}{dp_{\rm t_1}^2}\, \frac{d\sigma_{I_2J_2}^{2\to 2}}{dp_{\rm t_2}^2}$$
$$\times \int d^2\Delta\!\!\!/b\, F^{(2)}_{I_1I_2}(x_1^+, x_2^+, M_{\rm F_1}^2, M_{\rm F_2}^2, \Delta\!\!\!/b)$$
$$\times F^{(2)}_{J_1J_2}(x_1^-, x_2^-, M_{\rm F_1}^2, M_{\rm F_2}^2, \Delta\!\!\!/b)\,. \quad (3)$$

In the simplest approach, one neglects multiparton correlations and expresses $_2$GPDs as a convolution of generalized parton distributions (GPDs) for two independent partons:

$$F^{(2)}_{I_1I_2}(x_1, x_2, q_1^2, q_2^2, \Delta\!\!\!/b)$$
$$= \int d^2b'\, G_{I_1}(x_1, q_1^2, b')\, G_{I_2}(x_2, q_2^2, |\vec{b'} - \vec{\Delta\!\!\!/b}|)\,. \quad (4)$$

Without a loss of generality, we may express G_I via the usual PDFs $f_I(x, q^2)$ and the parton distribution in transverse space ρ_I as

$$G_I(x, q^2, b) = f_I(x, q^2)\, \rho_I(b, x, q^2)\,, \quad (5)$$

with $\int d^2b\, \rho_I(b, x, q^2) = 1$. One can thus cast the respective "(2v2)" contribution to $\sigma_{pp}^{\rm 4jet(DPS)}$ in the form [5]

$$\sigma_{pp}^{\rm 4jet(2v2)}(s, p_{\rm t}^{\rm cut}) = \frac{1}{2}\int d^2b$$
$$\times \left[\int dx^+ dx^- \int_{p_{\rm t} > p_{\rm t}^{\rm cut}} dp_{\rm t}^2 \sum_{I,J} f_I(x^+, M_{\rm F}^2)\right.$$
$$\left.\times\, f_J(x^-, M_{\rm F}^2)\, \frac{d\sigma_{IJ}^{2\to 2}}{dp_{\rm t}^2}\, \Omega_{IJ}(x^+, x^-, M_{\rm F}^2, b)\right]^2. \quad (6)$$

[1] Here and in the following we use $_2$GPDs in the impact parameter space, which are related to the ones introduced in Refs. [9, 10] via a Fourier transform.

Here

$$\Omega_{IJ}(x^+, x^-, M_{\rm F}^2, b) = \int d^2b'\, \rho_I(b', x^+, M_{\rm F}^2)$$
$$\times \rho_J(|\vec{b} - \vec{b'}|, x^-, M_{\rm F}^2) \quad (7)$$

are parton transverse overlap functions. In particular, assuming a simple universal Gaussian distribution for all partons,

$$\rho_I(b, x, q^2) = \tilde{\rho}(b) = \frac{1}{\pi R_p^2}\, e^{-b^2/R_p^2}\,, \quad (8)$$

one obtains for the respective effective cross section $\sigma_{pp}^{\rm eff(2v2)} = 4\pi R_p^2$, i.e. $\sigma_{pp}^{\rm eff(2v2)}$ is related to the effective area occupied by partons in the proton.

In reality, one has to take into consideration Gribov's transverse diffusion which produces a larger transverse spread for partons at smaller x [17, 18]. Moreover, as follows from simple dimensional considerations and is supported by HERA data [19, 20], the rate of the transverse diffusion is slower for partons of larger virtuality [21]. Thus, one expects $\sigma_{pp}^{\rm eff(2v2)}$ to increase with s due to the longer rapidity range available for the parton evolution, resulting in a larger transverse spread, and to decrease with $p_t^{\rm cut}$, due to a smaller part of the parton cascade developing in the low-q^2 region.

Recently, it has been demonstrated that substantial corrections to this simple picture arise from parton correlations induced by a perturbative parton splitting [9, 10, 11, 12, 14, 22]. In the latter case, two (say, projectile) partons participating in the two hard processes are no longer independent but emerge from the same "parent" parton of relatively high virtuality $|q^2| > Q_0^2 \gg \Lambda_{\rm QCD}^2$ and are close to each other in the transverse plane. The respective "$(2{\rm v}1)_{\rm h}$" contribution to $\sigma_{pp}^{\rm 4jet(DPS)}$ can be defined as [9, 10, 11, 12, 14]

$$\sigma_{pp}^{{\rm 4jet}(2{\rm v}1)_{\rm h}}(s, p_{\rm t}^{\rm cut}) = \frac{1}{2}\sum_L \int \frac{dx}{x^2} \int_{q^2 > Q_0^2} \frac{dq^2}{q^2}$$
$$\times f_L(x, q^2)\, \frac{\alpha_{\rm s}}{2\pi} \sum_K \int \frac{dz}{z(1-z)}\, P^{\rm AP}_{L\to K(K')}(z)$$
$$\times \int dx_1^+ dx_2^+ dx_1^- dx_2^- \int_{p_{\rm t_1}, p_{\rm t_2} > p_{\rm t}^{\rm cut}} dp_{\rm t_1}^2\, dp_{\rm t_2}^2$$
$$\times \sum_{I_1,I_2,J_1,J_2} E_{K\to I_1}(\frac{x_1^+}{zx}, q^2, M_{\rm F_1}^2)$$

$$\times E_{K'\to I_2}(\frac{x_2^+}{(1-z)x}, q^2, M_{\mathrm{F}_2}^2)\,\frac{d\sigma_{I_1J_1}^{2\to 2}}{dp_{\mathrm{t}_1}^2}\,\frac{d\sigma_{I_2J_2}^{2\to 2}}{dp_{\mathrm{t}_2}^2}$$
$$\times \int d^2b\, G_{J_1}(x_1^-, M_{\mathrm{F}_1}^2, b)\, G_{J_2}(x_2^-, M_{\mathrm{F}_2}^2, b)\,, \quad (9)$$

where $P^{\mathrm{AP}}_{I\to J(J')}$ is the Altarelli-Parisi splitting kernel and $E_{I\to J}(z, q^2, Q^2)$ is the solution of the DGLAP equations with the initial condition $E_{I\to J}(z, q^2, q^2) = \delta_I^J\,\delta(1-z)$, which describes parton evolution from the scale q^2 to Q^2. Despite being suppressed by an additional power of α_{s}, this contribution receives strong collinear enhancements [9, 10] and, for sufficiently high $p_{\mathrm{t}}^{\mathrm{cut}}$ and $Q_0 \sim 1$ GeV, appears to be comparable to $\sigma_{pp}^{4\mathrm{jet(2v2)}}$, thus reducing the effective cross section [Eq. (1)] by a factor of 2 [11, 23]. Implementing the mechanism in the PYTHIA Monte Carlo generator allows one to obtain a consistent description of multiparton interactions both for high p_t jet production and in underlying events [24].

For decreasing $p_{\mathrm{t}}^{\mathrm{cut}}$, the contribution of the perturbative parton splitting goes down due to the reduced kinematic space for the parton evolution. However, as suggested in [11, 25], additional important corrections to the DPS cross section should arise from nonperturbative parton correlations, e.g. ones related to nonperturbative parton splitting at $|q^2| < Q_0^2$. It is the goal of the present work to estimate the magnitude of such corrections, using a phenomenological Reggeon field theory (RFT) [26] approach. In Section 2, we describe the treatment of double parton scattering in the enhanced Pomeron framework, as implemented in the QGSJET-II model [27, 28]. In Section 3, we present some numerical results and discuss the obtained energy and p_t dependence of the DPS cross sections. Finally, we conclude in Section 4.

2 Double parton scattering in the enhanced Pomeron framework

We are going to investigate DPS using the enhanced Pomeron framework [29, 30, 31], as implemented in the QGSJET-II model [27, 28]. The approach takes into consideration the contributions of Pomeron-Pomeron interaction (so-called enhanced) diagrams. At the parton level, such graphs describe the rescattering of intermediate partons in the parton cascades off the parent hadrons and off each other.

To obtain a coherent treatment of both "soft" and "hard" interaction processes, general parton cascades are split into two parts, as described in more detail in Refs. [32, 33, 34]. The hard part is characterized by high enough parton virtualities $|q^2| > Q_0^2$, Q_0 being some cut-off for pQCD being applicable, and is treated by means of the DGLAP evolution equations. In turn, the nonperturbative soft part involves low-q^2 ($|q^2| < Q_0^2$) partons and is described by a phenomenological soft Pomeron asymptotic.

To treat low mass diffraction and the related absorptive (inelastic screening) effects, one employs a Good-Walker-type [35] framework, considering the interacting protons to be represented by a superposition of a number of eigenstates which diagonalize the scattering matrix, characterized by different couplings to Pomerons [36]. The respective partonic interpretation is based on the color fluctuations picture [37], i.e. the representation of the proton wave function by a superposition of parton Fock states of different sizes. Fock states of larger transverse size are characterized by lower (more dilute) spatial parton densities, while more compact ones are more densely packed with partons. As will be demonstrated in the following, such color fluctuations have important consequences both for the total rate of double parton scattering and for the relative importance of the different DPS contributions.

Let us start with the inclusive cross section for high transverse momentum ($p_{\mathrm{t}} > p_{\mathrm{t}}^{\mathrm{cut}}$) jet production, which is described by Kancheli-Mueller-type diagrams depicted in Fig. 1. The internal structure of the projectile and target "triangles" of Fig. 1 is explained in Fig. 2. The basic contribution is a single Pomeron emission by the parent hadron [1st graph in the rhs of Fig. 2], which corresponds to an "elementary" parton cascade. Absorptive corrections to that process involve Pomeron-Pomeron interactions and arise from the rescattering of intermediate partons in the cascade off the parent hadron (2nd, 3rd, and 4th graphs in the rhs) and off each other (5th graph in the rhs).

Neglecting absorptive corrections due to enhanced Pomeron diagrams, the inclusive cross section $\sigma_{pp}^{2\mathrm{jet(no\,abs)}}(s, p_{\mathrm{t}}^{\mathrm{cut}})$ for the production of

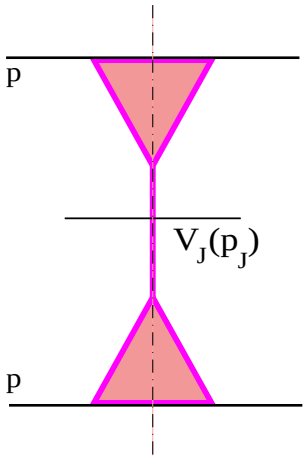

Figure **1**: Schematic view for the general RFT diagram for inclusive jet production in pp collisions: the projectile and target triangles consist of fanlike enhanced Pomeron graphs; $V_J(p_J)$ is the parton J emission vertex from a cut Pomeron. The cut plane is shown by the vertical dotted-dashed line.

a pair of jets of transverse momentum $p_{\rm t} > p_{\rm t}^{\rm cut}$ is defined as [33, 34]

$$\sigma_{pp}^{\rm 2jet(no\,abs)}(s,p_{\rm t}^{\rm cut}) = \sum_{i,j} C_i\,C_j \int d^2b'\,d^2b'' \times \int \frac{dx^+}{x^+}\frac{dx^-}{x^-} \sum_{I,J} \chi_{(i)I}^{\mathbb{P}_{\rm soft}}(s_0/x^+,b') \times \chi_{(j)J}^{\mathbb{P}_{\rm soft}}(s_0/x^-,b'')\,\sigma_{IJ}^{\rm QCD}(x^+x^-s,Q_0^2,p_{\rm t}^{\rm cut})\,, \quad (10)$$

where

$$\sigma_{IJ}^{\rm QCD}(x^+x^-s,Q_0^2,p_{\rm t}^{\rm cut}) = \int_{p_{\rm t}>p_{\rm t}^{\rm cut}} dp_{\rm t}^2 \times \int dz^+dz^- \sum_{I',J'} \frac{d\sigma_{I'J'}^{2\to2}(x^+x^-z^+z^-s,p_t^2)}{dp_{\rm t}^2} \times E_{I\to I'}(z^+,Q_0^2,M_{\rm F}^2)\,E_{J\to J'}(z^-,Q_0^2,M_{\rm F}^2) \quad (11)$$

is the contribution of the DGLAP ladder, corresponding to the production of a pair of jets of $p_{\rm t} > p_{\rm t}^{\rm cut}$, with ladder leg partons of types I, J [sea (anti)quarks or gluons[2]], characterized by the virtuality Q_0^2 and fractions x^+, x^- of the parent hadrons' light-cone momenta. In turn, $\chi_{(i)I}^{\mathbb{P}_{\rm soft}}$ is the eikonal describing a soft Pomeron exchange between the parent proton represented by its diffractive eigenstate $|i\rangle$ and the ladder leg parton I;

$$\chi_{(i)I}^{\mathbb{P}_{\rm soft}}(\hat{s},b) \propto \frac{\lambda_i\,\hat{s}^{\alpha_{\mathbb{P}}-1}}{R_i^2+\alpha'_{\mathbb{P}}\,\ln\hat{s}}\,e^{-\frac{b^2}{4(R_i^2+\alpha'_{\mathbb{P}}\,\ln\hat{s})}} \quad (12)$$

for sufficiently large $\hat{s}$; $\alpha_{\mathbb{P}}$ and $\alpha'_{\mathbb{P}}$ are, respectively, the intercept and the slope of the soft Pomeron Regge trajectory. C_i is the partial weight of Fock state $|i\rangle$ while λ_i and R_i^2 are the relative strength and the slope for Pomeron coupling to $|i\rangle$, $\sum_i C_i\,\lambda_i = 1$.

Including absorptive corrections due to enhanced Pomeron graphs but neglecting for simplicity contributions of Pomeron loop diagrams (of the kind of the 5th graph in the rhs of Fig. 2), which prove not to be essential in the kinematic range studied in this work, the projectile and target triangles in Fig. 1 consist of "fanlike" Pomeron graphs (examples of contributions of lowest orders are 1st, 2nd, 3rd, and 4th graphs in the rhs of Fig. 2). Thus, Eq. (10) transforms to [27]

$$\sigma_{pp}^{\rm 2jet}(s,p_{\rm t}^{\rm cut}) = \sum_{i,j} C_i\,C_j \int d^2b'\,d^2b'' \times \int dx^+\,dx^- \sum_{I,J} \tilde{f}_I^{(i)}(x^+,b')\,\tilde{f}_J^{(j)}(x^-,b'') \times \sigma_{IJ}^{\rm QCD}(x^+x^-s,Q_0^2,p_{\rm t}^{\rm cut})\,, \quad (13)$$

with

$$x\,\tilde{f}_I^{(i)}(x,b) = \chi_{(i)I}^{\mathbb{P}_{\rm soft}}(s_0/x,b) + G\int d^2b' \int \frac{dx'}{x'} \times \left[1-e^{-\chi_{(i)}^{\rm fan}(s_0/x',b')} - \chi_{(i)}^{\rm fan}(s_0/x',b')\right] \times \chi_{\mathbb{P}I}^{\mathbb{P}_{\rm soft}}(s_0\,x'/x,|\vec{b}-\vec{b}'|)\,. \quad (14)$$

Here $\chi_{(i)}^{\rm fan}$ is the solution of the fan diagram equation

$$\chi_{(i)}^{\rm fan}(\hat{s},b) = \chi_{(i)\mathbb{P}}^{\mathbb{P}_{\rm soft}}(\hat{s},b) + G\int d^2b' \int \frac{dx'}{x'} \times \left[1-e^{-\chi_{(i)}^{\rm fan}(s_0/x',b')} - \chi_{(i)}^{\rm fan}(s_0/x',b')\right] \times \chi_{\mathbb{P}\mathbb{P}}^{\mathbb{P}_{\rm soft}}(x'\hat{s},|\vec{b}-\vec{b}'|)\,, \quad (15)$$

where the eikonal $\chi_{(i)\mathbb{P}}^{\mathbb{P}_{\rm soft}}(\hat{s},b)$ corresponds to soft Pomeron exchange between proton's diffractive eigenstate $|i\rangle$ and a multi-Pomeron vertex, which depends on $\hat{s}$, b, λ_i, R_i^2 like $\chi_{(i)I}^{\mathbb{P}_{\rm soft}}$ in Eq. (12).

[2]For brevity, we shall not discuss explicitly valence quark contributions, which are of secondary importance for the present analysis.

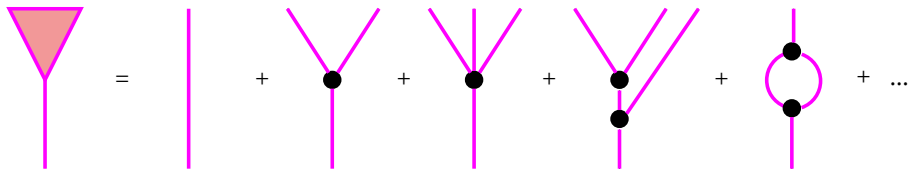

Figure **2**: Examples of enhanced Pomeron graphs of lowest orders, contributing to the structure of the projectile and target triangles in Fig. 1; Pomerons are shown by thick lines and multi-Pomeron vertices by filled circles.

$\chi_{\mathbb{P}\mathbb{P}}^{\mathbb{P}_{\rm soft}}$ describes soft Pomeron exchange between two multi-Pomeron vertices,

$$\chi_{\mathbb{P}\mathbb{P}}^{\mathbb{P}_{\rm soft}}(\hat{s},b) = \frac{\gamma_{\mathbb{P}}^2\,\hat{s}^{\alpha_{\mathbb{P}}-1}}{\alpha'_{\mathbb{P}}\,\ln\hat{s}}\,e^{-\frac{b^2}{4\alpha'_{\mathbb{P}}\,\ln\hat{s}}}\,. \qquad (16)$$

The eikonal $\chi_{\mathbb{P}I}^{\mathbb{P}_{\rm soft}}$, corresponding to a Pomeron exchanged between a multi-Pomeron vertex and parton I, is obtained from $\chi_{\mathbb{P}\mathbb{P}}^{\mathbb{P}_{\rm soft}}$ replacing one factor $\gamma_{\mathbb{P}}$ by a Pomeron-parton vertex, as discussed in more detail in Ref. [27]. It is noteworthy that Eqs. (13-15) have been derived in Ref. [27] neglecting parton transverse diffusion during the perturbative ($|q^2| > Q_0^2$) evolution and assuming the vertices for the transition of m into n Pomerons to be of the form [30]

$$G^{(m,n)} = G\,\gamma_{\mathbb{P}}^{m+n}. \qquad (17)$$

G is related to the triple-Pomeron vertex $r_{3\mathbb{P}}$ as $G = r_{3\mathbb{P}}/(4\pi\gamma_{\mathbb{P}}^3)$.

Comparing now Eqs. (13) and (11) with Eqs. (2) and (5), we may interpret $\tilde{f}_I^{(i)}(x,b)$ as GPDs $G_I^{(i)}(x,Q_0^2,b)$ of sea (anti)quarks and gluons at the virtuality scale Q_0^2 for the Fock state $|i\rangle$ [27]. Let us briefly discuss their x and b dependence. For sufficiently large b, absorptive corrections are weak and the respective low x behavior of $\tilde{f}_I^{(i)}$ is described by the soft Pomeron asymptotic, $\tilde{f}_I^{(i)}(x,b) \propto x^{-\alpha_{\mathbb{P}}}$ for $x \to 0$ [cf. Eqs. (14) and (12)]. For decreasing b, absorptive corrections become stronger, producing parton shadowing effects. At sufficiently small x, one approaches the flat $x\,\tilde{f}_I^{(i)}(x,b) \simeq$ const behavior for $b \simeq 0$ [38]. Let us turn now to the parton spatial distribution. Because of the transverse diffusion during the soft ($|q^2| < Q_0^2$) parton cascade, governed by the soft Pomeron slope $\alpha'_{\mathbb{P}}$, smaller x partons are distributed over a larger transverse area [see Eq. (12)] at the scale Q_0^2. As the Pomeron slope is rather small, the difference between the effective radii of the parton spatial distributions for different Fock states, caused by the different slopes R_i^2, should persist down to rather small values of x, being gradually washed out by the transverse diffusion. It is noteworthy that absorptive corrections produce stronger shadowing at smaller impact parameters and for smaller x, as already discussed above, which effectively speeds up the diffusion process.[3]

GPDs at a higher scale $Q^2 > Q_0^2$ are obtained by evolving the input ones (as mentioned above, we neglect parton transverse diffusion at $|q^2| > Q_0^2$):

$$G_I^{(i)}(x,Q^2,b) = \sum_{I'}\int_x^1 \frac{dz}{z}\,E_{I'\to I}(z,Q_0^2,Q^2) \times \tilde{f}_{I'}^{(i)}(x/z,b)\,. \qquad (18)$$

Thus, the available rapidity range $\Delta y = \ln(1/x)$ is shared between the soft ($|q^2| < Q_0^2$) and the hard parton evolution; the larger the Q^2, the shorter the soft part. As a consequence, for a given x, partons of higher Q^2 are distributed over a smaller transverse area.

Let us now turn to the DPS contribution to double dijet production. We start with the graph in Fig. 3(a) where the pair of projectile (respectively, target) partons participating in the two hard processes originates from independent parton cascades. This leads us to

$$\sigma_{pp}^{4{\rm jet(2v2)}}(s,p_{\rm t}^{\rm cut}) = \frac{1}{2}\sum_{i,j} C_i\,C_j \int d^2b \times \left[\int dx^+\,dx^-\sum_{I,J}\sigma_{IJ}^{\rm QCD}(x^+x^-s,Q_0^2,p_{\rm t}^{\rm cut}) \times \int d^2b'\,\tilde{f}_I^{(i)}(x^+,b')\,\tilde{f}_J^{(j)}(x^-,|\vec{b}-\vec{b}'|)\right]^2. \qquad (19)$$

[3] Such an effect has been discussed previously in Ref. [39].

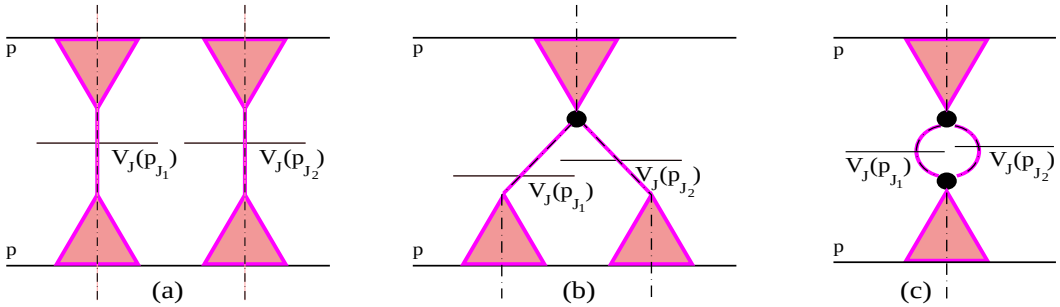

Figure **3**: Schematic view of RFT diagrams for double parton scattering: contribution of two independent parton cascades (a), projectile parton splitting (b), and double parton splitting (c).

Interpreting $\tilde{f}_I^{(i)}(x,b)$ as GPDs at the scale Q_0^2, Eq. (19) is similar to Eq. (6) with one important difference: the pair of projectile (respectively, target) partons participating in the hard processes is not actually uncorrelated. Indeed, $\sigma_{pp}^{4\mathrm{jet(2v2)}}$ in Eq. (19) is obtained by averaging over contributions of different Fock states. Most importantly, in Fock states with the smallest R_i^2, partons are more closely packed together, which enhances the respective contributions to $\sigma_{pp}^{4\mathrm{jet(2v2)}}$. On the other hand, for increasing s, the effect is slowly washed out due to the parton transverse diffusion.

Next, we consider the "soft splitting" contribution "$(2\mathrm{v}1)_{\mathrm{s}}$" of Fig. 3(b), for which we obtain (neglecting Pomeron loop corrections)

$$\sigma_{pp}^{4\mathrm{jet}(2\mathrm{v}1)_{\mathrm{s}}}(s,p_{\mathrm{t}}^{\mathrm{cut}}) = \frac{1}{2}\sum_{i,j} C_i\, C_j \int d^2b' \int \frac{dx'}{x'} \times G\left[1-e^{-\chi_{(i)}^{\mathrm{fan}}(s_0/x',b')}\right] \int d^2b \left[\int \frac{dx^+}{x^+} \times \int dx^- \int d^2b'' \sum_{I,J} \chi_{\mathbb{P}I}^{\mathbb{P}_{\mathrm{soft}}}(s_0\, x'/x^+, b'') \times \tilde{f}_J^{(j)}(x^-, |\vec{b}-\vec{b}''|)\, \sigma_{IJ}^{\mathrm{QCD}}(x^+x^-s, Q_0^2, p_{\mathrm{t}}^{\mathrm{cut}})\right]^2 . \quad (20)$$

It is noteworthy that the (2v2) [Eq. (19)] and the two (projectile and target parton splitting) $(2\mathrm{v}1)_{\mathrm{s}}$ [Eq. (20)] contributions can be obtained from Eq. (3) if ${}_2$GPDs at the scale Q_0^2 are defined as

$$F_{I_1I_2}^{(2)}(x_1,x_2,Q_0^2,Q_0^2,\Delta b) = \sum_i C_i \int d^2b' \left\{ \tilde{f}_{I_1}^{(i)}(x_1,b')\, \tilde{f}_{I_2}^{(i)}(x_2,|\vec{b}'-\vec{\Delta b}|) + \frac{G}{x_1x_2}\int \frac{dx'}{x'}\left[1-e^{-\chi_{(i)}^{\mathrm{fan}}(s_0/x',b')}\right]\int d^2b'' \times \chi_{\mathbb{P}I_1}^{\mathbb{P}_{\mathrm{soft}}}(s_0x'/x_1,b'')\, \chi_{\mathbb{P}I_2}^{\mathbb{P}_{\mathrm{soft}}}(s_0x'/x_2,|\vec{b}''-\vec{\Delta b}|)\right\} \quad (21)$$

and the two branches of the cascade are separately evolved from Q_0^2 to q_1^2, q_2^2:

$$F_{I_1I_2}^{(2)}(x_1,x_2,q_1^2,q_2^2,\Delta b) = \sum_{J_1,J_2}\int_{x_1}^1 \frac{dz_1}{z_1}\int_{x_2}^1 \frac{dz_2}{z_2} \times E_{J_1\to I_1}(z_1,Q_0^2,q_1^2)\, E_{J_2\to I_2}(z_2,Q_0^2,q_2^2) \times F_{J_1J_2}^{(2)}(x_1/z_1,x_2/z_2,Q_0^2,Q_0^2,\Delta b)\,. \quad (22)$$

In addition, such a substitution would generate the loop contribution of Fig. 3(c), which is neglected in the present analysis (the respective correction appears to be at the few percent level).

Finally, we have to add the perturbative parton splitting $(2\mathrm{v}1)_{\mathrm{h}}$ contribution, which is not included in the present QGSJET-II model.[4] Interpreting $\tilde{f}_I^{(i)}(x,b)$ as partial GPDs at the scale Q_0^2, we obtain, similarly to Eq. (9),

$$\sigma_{pp}^{4\mathrm{jet}(2\mathrm{v}1)_{\mathrm{h}}}(s,p_{\mathrm{t}}^{\mathrm{cut}}) = \frac{1}{2}\sum_{i,j} C_i\, C_j \int_{q^2>Q_0^2}\frac{dq^2}{q^2} \times \int \frac{dx}{x^2}\int d^2b' \sum_L G_L^{(i)}(x,q^2,b') \int \frac{dz}{z(1-z)} \times \frac{\alpha_{\mathrm{s}}}{2\pi}\sum_K P_{L\to K(K')}^{\mathrm{AP}}(z) \int dx_1^+ dx_2^+ dx_1^- dx_2^- \times \int_{p_{\mathrm{t}_1},p_{\mathrm{t}_2}>p_{\mathrm{t}}^{\mathrm{cut}}} dp_{\mathrm{t}_1}^2\, dp_{\mathrm{t}_2}^2 \sum_{I_1,I_2,J_1,J_2} \frac{d\sigma_{I_1J_1}^{2\to2}}{dp_{\mathrm{t}_1}^2}\frac{d\sigma_{I_2J_2}^{2\to2}}{dp_{\mathrm{t}_2}^2} \times E_{K\to I_1}(x_1^+/x/z,q^2,M_{\mathrm{F}_1}^2)$$

[4] The respective RFT treatment was based on phenomenological multi-Pomeron vertices (17), assuming that Pomeron-Pomeron coupling is dominated by parton processes at low $|q^2| < Q_0^2$.

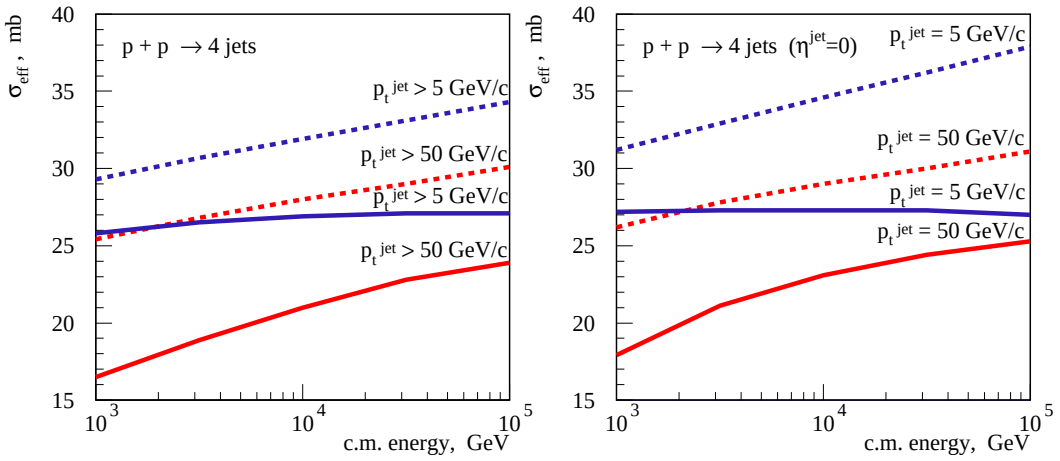
σ_eff , mb
p + p → 4 jets
p_t^jet > 5 GeV/c
p_t^jet > 50 GeV/c
p_t^jet > 5 GeV/c
p_t^jet > 50 GeV/c
c.m. energy, GeV
p + p → 4 jets (η^jet=0)
p_t^jet = 5 GeV/c
p_t^jet = 50 GeV/c
p_t^jet = 5 GeV/c
p_t^jet = 50 GeV/c
c.m. energy, GeV

Figure **4**: Energy dependence of the effective cross section for the production of two dijets in double parton scattering. Left: for jet transverse momenta $p_{\rm t}^{\rm jet} > 5$ GeV/c and $p_{\rm t}^{\rm jet} > 50$ GeV/c (as indicated in the plots), integrated over the phase space. Right: for fixed $p_{\rm t}^{\rm jet} = 5$ and 50 GeV/c and $\eta^{\rm jet} = 0$. Solid lines - both the (2v2) and (2v1) contributions to DPS taken into account, dashed lines - only the (2v2) contribution considered.

$$\times E_{K'\to I_2}(x_2^+/x/(1-z), q^2, M_{\rm F_2}^2)$$
$$\times \int d^2b\, G_{J_1}^{(j)}(x_1^-, M_{\rm F_1}^2, b)\, G_{J_2}^{(j)}(x_2^-, M_{\rm F_2}^2, b)\,, \quad (23)$$

where $G_I^{(i)}(x, Q^2, b)$ is defined by Eq. (18).

Because of the smallness of the Pomeron slope $\alpha'_{\mathbb{P}}$, the soft splitting contribution $(2{\rm v}1)_{\rm s}$ of Eq. (20) bears some similarity to the one of perturbative splitting [Eq. (23)]: the two projectile partons participating in the two hard processes are close by in the transverse plane [the integral over b'' in Eq. (20) is dominated by the small $b'' \ll b$ region, cf. Eq. (16)]. In other words, the second term in the curly brackets in the rhs of Eq. (21) generates short range correlations between the two partons in coordinate space.

In the next section, we apply Eqs. (13), (19), (20), and (23) to investigate the energy and transverse momentum dependence of the partial DPS cross sections for the production of two dijets and of the respective effective cross sections. We shall use the parameter set of the QGSJET-II-04 model [28], which has been obtained by fitting the model to available accelerator data on the total and elastic proton-proton cross sections, elastic scattering slope, and total and diffractive structure functions F_2, $F_2^{\rm D(3)}$. In particular, we consider two diffractive eigenstates with equal weights, $C_1 = C_2 = 1/2$, with the relative strengths $\lambda_1 = 1.6$, $\lambda_2 = 0.4$, and with the slopes $R_1^2 = 2.5\ {\rm GeV}^{-2}$, $R_2^2 = 0.2\ {\rm GeV}^{-2}$; the Pomeron intercept, slope, and the triple-Pomeron coupling are, respectively, $\alpha_{\mathbb{P}} = 1.17$, $\alpha'_{\mathbb{P}} = 0.14\ {\rm GeV}^{-2}$, and $r_{3\mathbb{P}} = 0.1$ GeV. For the "soft-hard" separation scale, we use $Q_0^2 = 3\ {\rm GeV}^2$ and the factorization scale in Eq. (11) is chosen as $M_{\rm F}^2 = p_t^2/4$.

3 Results and discussion

Let us start with the investigation of the energy dependence of the effective cross section for the production of two hadronic dijets in double parton scattering. In Fig. 4 (left), we plot by solid lines $\sigma_{pp}^{\rm eff}$ for the production of jets of transverse momenta $p_{\rm t}^{\rm jet} > p_{\rm t}^{\rm cut}$ for two choices of $p_{\rm t}^{\rm cut}$, integrated over the phase space. More specifically, $\sigma_{pp}^{\rm eff}$ is calculated according to Eq. (1), taking into account all the discussed contributions to $\sigma_{pp}^{\rm 4jet(DPS)}$, i.e.

$$\sigma_{pp}^{\rm eff}(s, p_{\rm t}^{\rm cut}) = \frac{1}{2}\,\frac{\left[\sigma_{pp}^{\rm 2jet}(s, p_{\rm t}^{\rm cut})\right]^2}{\sum_\alpha \sigma_{pp}^{\rm 4jet(\alpha)}(s, p_{\rm t}^{\rm cut})}\,, \quad (24)$$

where $\alpha = (2{\rm v}2), (2{\rm v}1)_{\rm s}, (2{\rm v}1)_{\rm h}$. The corresponding cross sections $\sigma_{pp}^{\rm 4jet(2v2)}$, $\sigma_{pp}^{\rm 4jet(2v1)_s}$, and $\sigma_{pp}^{\rm 4jet(2v1)_h}$ are defined by Eqs. (19), (20), and (23), respectively, with the latter two contributions being multiplied by factor of 2 to ac-

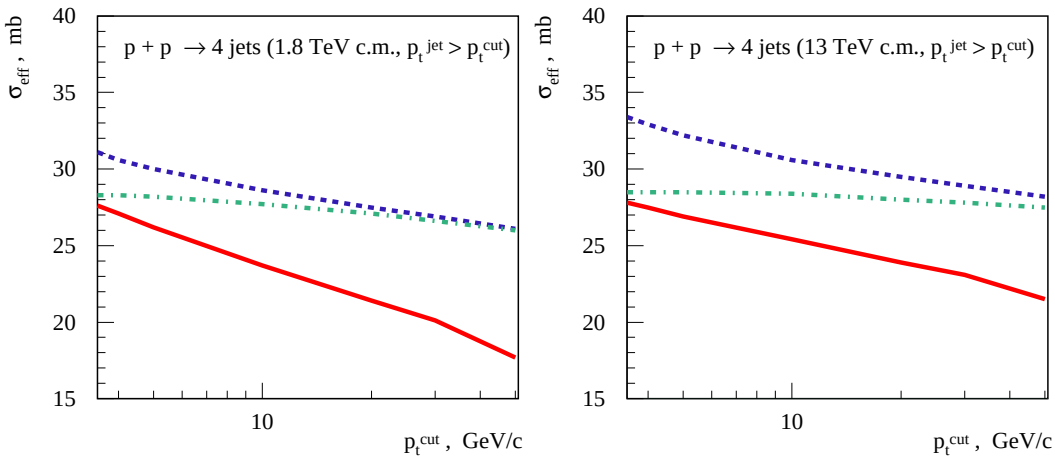

Figure **5**: Effective cross section for the production of two dijets of $p_{\rm t}^{\rm jet} > p_{\rm t}^{\rm cut}$, integrated over the phase space, in double parton scattering at $\sqrt{s} = 1.8$ TeV (left) and $\sqrt{s} = 13$ TeV (right) as a function of $p_{\rm t}^{\rm cut}$: solid - all the DPS contributions taken into account, dashed - only the (2v2) contribution considered, dotted-dashed - including both the (2v2) and $(2{\rm v}1)_{\rm s}$ contributions.

count for the possibility of parton splitting both on the projectile and target sides. In addition, we show by dashed lines the effective cross section as obtained by considering the simplest (2v2) DPS configuration only, $\sigma_{pp}^{\rm eff(2v2)} = \frac{1}{2}\left[\sigma_{pp}^{\rm 2jet}\right]^2/\sigma_{pp}^{\rm 4jet(2v2)}$. For comparison with earlier studies, we repeat the above calculations for the case of central ($\eta = 0$) production of a pair of dijets of fixed transverse momentum $p_{\rm t}^{\rm jet}$, the results being plotted in Fig. 4 (right).

Looking first at $\sigma_{pp}^{\rm eff(2v2)}$ shown by the dashed lines in Fig. 4, we clearly see the trends discussed in the Introduction and already observed in previous studies [11, 23]: the respective effective cross section increases with $\sqrt{s}$ and decreases with jet $p_{\rm t}$. The energy rise is due to the increasing rapidity interval for the parton evolution, hence, also an extended rapidity range for the soft ($|q^2| < Q_0^2$) evolution, which results in a larger parton transverse spread. The decrease of $\sigma_{pp}^{\rm eff}$ with increasing jet $p_{\rm t}$ for the same $\sqrt{s}$ is caused by a reduction of the soft part of the parton evolution. Indeed, configurations with a larger part of the parton cascade developing in the hard ($|q^2| > Q_0^2$) regime have stronger (double logarithmic) enhancement, thus winning over the ones characterized by a longer soft part. In turn, shorter soft evolution produces a smaller transverse spread of partons and leads to a smaller effective cross section.

Interestingly, for sufficiently large $p_{\rm t}^{\rm jet}$ the obtained values of $\sigma_{pp}^{\rm eff(2v2)}$ are noticeably reduced relative to the results of Refs. [11, 23]. For example, for central production of two dijets at $\sqrt{s} = 1.8$ TeV, we obtain $\sigma_{pp}^{\rm eff(2v2)} \simeq 27$ mb for $p_{\rm t}^{\rm jet} = 50$ GeV/c, to be compared to $\simeq 30 - 32$ mb in Refs. [11, 23]. This reduction is caused by averaging over the contributions of different Good-Walker Fock states in Eq. (19), which corresponds to averaging over color fluctuations in the interacting protons. Indeed, the effective cross section is very sensitive to contributions of parton Fock states of small transverse size, which are characterized by a higher spatial parton density and correspondingly by a larger DPS rate, as discussed previously in Refs. [37, 40]. In other words, the discussed reduction of $\sigma_{pp}^{\rm eff(2v2)}$ is caused by additional correlations in parton spatial distributions, which are generated by color fluctuations, compared to the simple factorization ansatz of Eq. (4).

Let us now turn to $\sigma_{pp}^{\rm eff}$ calculated with the soft and hard parton splittings taken into account, shown by the solid lines in Fig. 4. Here we observe that the above-discussed energy and jet transverse momentum dependencies are substantially reduced in the very high energy limit. This is also clearly seen in Fig. 5, where we show the $p_{\rm t}^{\rm cut}$ dependence of the effective cross section for the production of a pair of dijets of

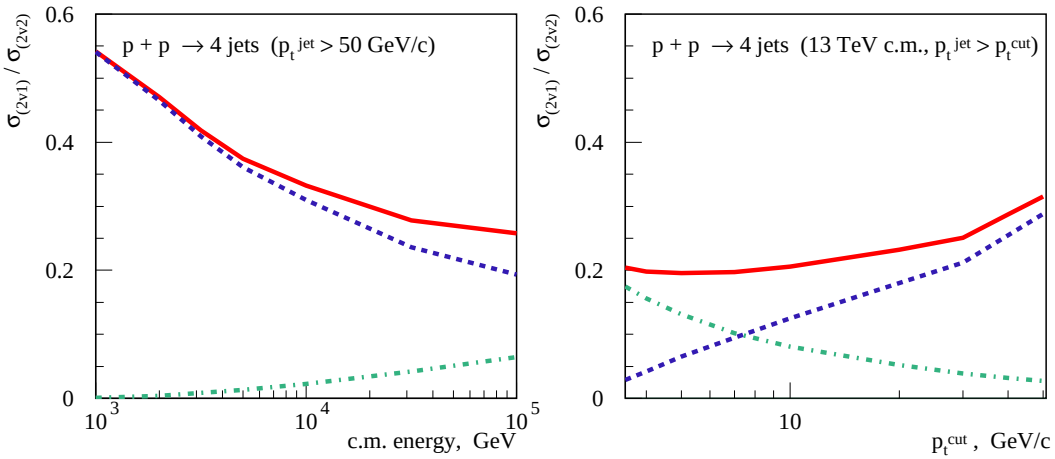

Figure **6**: Energy dependence for $p_{\rm t}^{\rm cut} = 50$ GeV/c (left) and $p_{\rm t}^{\rm cut}$ dependence for $\sqrt{s} = 13$ TeV (right) of the ratio of the (2v1) to (2v2) contributions to the DPS cross section for double dijet ($p_{\rm t}^{\rm jet} > p_{\rm t}^{\rm cut}$) production (solid) and partial contributions to this ratio from hard (dashed) and soft (dotted-dashed) parton splitting mechanisms.

$p_{\rm t}^{\rm jet} > p_{\rm t}^{\rm cut}$ at the Tevatron and the present LHC energies. We compare again $\sigma_{pp}^{\rm eff}$ calculated with all the discussed contributions taken into account to the one based on the (2v2) mechanism only, $\sigma_{pp}^{\rm eff(2v2)}$. To investigate the relative importance of the soft and hard parton splittings, we show in Fig. 5 the effective cross sections calculated using the (2v2) and $(2{\rm v}1)_{\rm s}$ contributions, i.e., accounting for the nonperturbative parton splitting only (dotted-dashed lines). Our results nicely demonstrate how the two splitting mechanisms complement each other. While the contribution of the perturbative parton splitting decreases for $p_{\rm t}^{\rm cut} \to Q_0$ (the solid and dotted-dashed lines approach each other), the opposite applies to the respective nonperturbative contribution: it is quite small for high $p_{\rm t}^{\rm cut}$ but gradually increases with the decrease of the transverse momentum cutoff and provides the dominant correction to the simple (2v2) picture when approaching the $p_{\rm t}^{\rm cut} = Q_0$ value. As a result, the effective cross section obtained with both contributions taken into account is characterized by a relatively weak $p_t^{\rm cut}$ dependence, as anticipated previously in Refs. [11, 25] and indicated by experimental data [1, 2, 3, 4].

To investigate further the relative roles of the soft and hard parton splitting mechanisms, we plot in Fig. 6 the calculated $p_{\rm t}^{\rm cut}$ dependence (at $\sqrt{s} = 13$ TeV) and the energy dependence (for $p_{\rm t}^{\rm cut} = 50$ GeV/c) of the ratio of the (2v1) to (2v2) contributions to the DPS cross section for the production of two dijets of $p_{\rm t}^{\rm jet} > p_{\rm t}^{\rm cut}$, $\left[\sigma_{pp}^{4{\rm jet}(2{\rm v}1)_{\rm s}} + \sigma_{pp}^{4{\rm jet}(2{\rm v}1)_{\rm h}}\right]/\sigma_{pp}^{4{\rm jet}(2{\rm v}2)}$. The partial contributions to this ratio from soft, $\sigma_{pp}^{4{\rm jet}(2{\rm v}1)_{\rm s}}/\sigma_{pp}^{4{\rm jet}(2{\rm v}2)}$, and hard, $\sigma_{pp}^{4{\rm jet}(2{\rm v}1)_{\rm h}}/\sigma_{pp}^{4{\rm jet}(2{\rm v}2)}$, parton splittings are shown by dotted-dashed and dashed lines respectively. Additionally, in Fig. 7, we plot the energy and transverse momentum dependencies of the same quantities for central ($\eta = 0$) production of a pair of dijets for fixed $p_{\rm t}^{\rm jet}$. The plots in Fig. 6 (right) and Fig. 7 (right) clearly demonstrate the increasing importance of the contribution of the nonperturbative parton splitting when jet $p_{\rm t}$ decreases.

Let us now turn to the energy dependence of the relative contributions of soft and hard parton splittings to the (2v1) mechanism, shown in Fig. 6 (left) for the production of a pair of dijets of $p_{\rm t}^{\rm jet} > 50$ GeV/c, integrated over the phase space, and in Fig. 7 (left) for central production of two dijets of fixed $p_{\rm t}^{\rm jet} = 50$ GeV/c. The contribution of the nonperturbative parton splitting, plotted by dotted-dashed lines, exhibits a noticeable energy rise, which is mostly due to the increasing rapidity range available for parton evolution. In contrast, the relative contribution of the hard splitting is gradually reduced with increasing energy. This is mainly because the contribution of the perturbative parton splitting

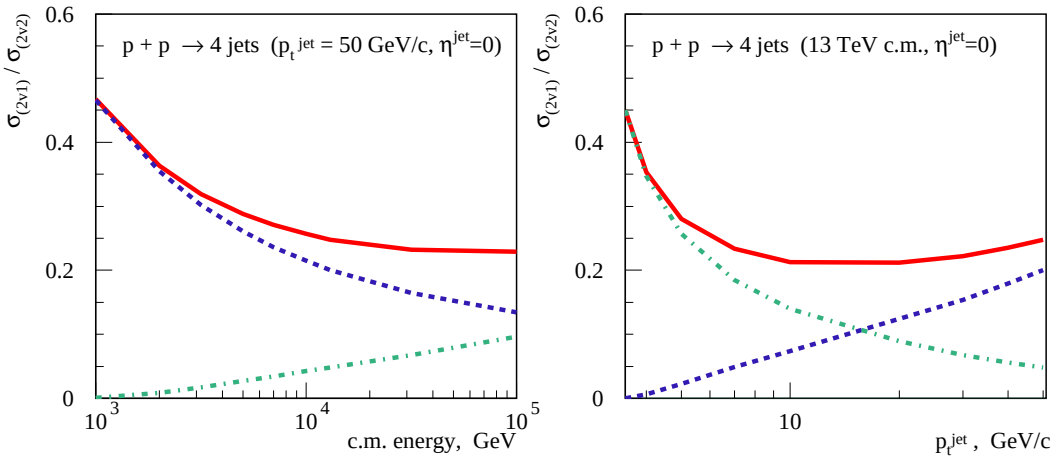

Figure **7**: Energy dependence for $p_{\rm t}^{\rm jet} = 50$ GeV/c (left) and $p_{\rm t}^{\rm jet}$ dependence for $\sqrt{s} = 13$ TeV (right) of the ratio of the (2v1) to (2v2) contributions to the DPS production of two dijets of fixed $p_{\rm t}^{\rm jet}$ for $\eta^{\rm jet} = 0$ (solid lines). Partial contributions to this ratio from hard and soft parton splitting mechanisms are shown by dashed and dotted-dashed lines, respectively.

to ${}_2$GPDs of gluons is effectively one $\ln x$ short in the low x limit, compared to the case of two independent parton cascades,[5] as discussed previously in Refs. [11, 25] (see, e.g., Fig. 2 in Ref. [25]). Apart from that, an additional reduction arises due to color fluctuations in the interacting protons and partons' transverse diffusion.

To elucidate this latter point, let us compare in Fig. 8 the energy dependence of the ratios

$$R^{(ii)}_{(2{\rm v}1)_{\rm h}} = \sigma^{4{\rm jet}(2{\rm v}1)_{\rm h}}_{(ii)} / \sigma^{4{\rm jet}(2{\rm v}2)}_{(ii)} \qquad (25)$$

of the $(2{\rm v}1)_{\rm h}$ to (2v2) contributions for combinations of large ($i = 1$) and small ($i = 2$) size diffractive eigenstates of the projectile and target protons, where $\sigma^{4{\rm jet}(2{\rm v}2)}_{(ii)}$ and $\sigma^{4{\rm jet}(2{\rm v}1)_{\rm h}}_{(ii)}$ are given by the corresponding terms (for fixed $i = j$) in the rhs of Eqs. (19) and (23) respectively. Obviously, the ratio $R^{(ii)}_{(2{\rm v}1)_{\rm h}}$ is much larger in the case of the small size parton configurations ($i = 2$), where the contribution of the perturbative splitting of, e.g., a projectile parton is strongly enhanced by the large spatial parton density in the target (or vice versa). The effects of parton diffusion are largely canceled[6] between the numerator and the denominator in Eq. (25), which results in a very similar energy dependence for $R^{(11)}_{(2{\rm v}1)_{\rm h}}$ and $R^{(22)}_{(2{\rm v}1)_{\rm h}}$. In contrast, the ratio of the total $(2{\rm v}1)_{\rm h}$ to (2v2) contribu-

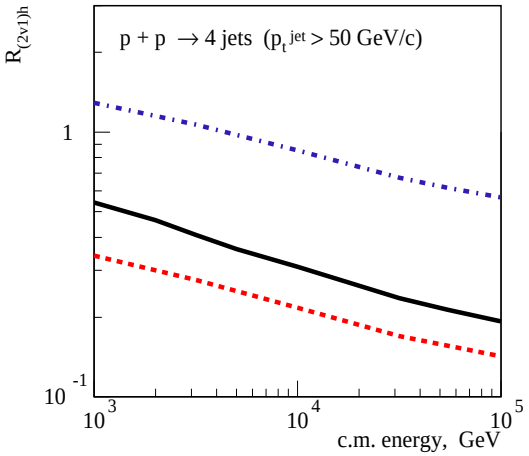

Figure **8**: Energy dependence of the ratio $R_{(2{\rm v}1)_{\rm h}}$ of the $(2{\rm v}1)_{\rm h}$ to (2v2) contributions to the DPS production of two dijets of $p_{\rm t}^{\rm jet} > 50$ GeV/c (solid line) and the ratios $R^{(ii)}_{(2{\rm v}1)_{\rm h}}$ for the combinations of large ($i = 1$) and small ($i = 2$) size parton Fock states - dashed and dotted-dashed lines, respectively.

[5] In the case of the hard parton splitting, there is a single convolution with the gluon PDF at the initial scale Q_0^2.

[6] In fact, such a cancellation is precise for central ($\eta = 0$) production of a dijet pair of fixed $p_{\rm t}^{\rm jet}$.

tions,

$$R_{(2v1)_h} = \left[\sum_{i,j} \sigma_{(ij)}^{4jet(2v1)_h}\right] / \left[\sum_{i,j} \sigma_{(ij)}^{4jet(2v2)}\right], \quad (26)$$

shown by the solid line in Fig. 8, falls down faster with increasing energy. This is because the effects of parton diffusion are particularly important for the small-size Fock states, leading to a fast increase of the effective radius of low-x parton clouds (compared to the spatial distribution of large-x partons) and to a quick energy decrease of the respective contributions, $\sigma_{(22)}^{4jet(2v2)}$ and $\sigma_{(22)}^{4jet(2v1)_h}$ (and similarly for the off-diagonal contributions, $\sigma_{(12)}^{4jet(2v2)}$ and $\sigma_{(12)}^{4jet(2v1)_h}$). We illustrate the latter point by comparing in Fig. 9 the ratios

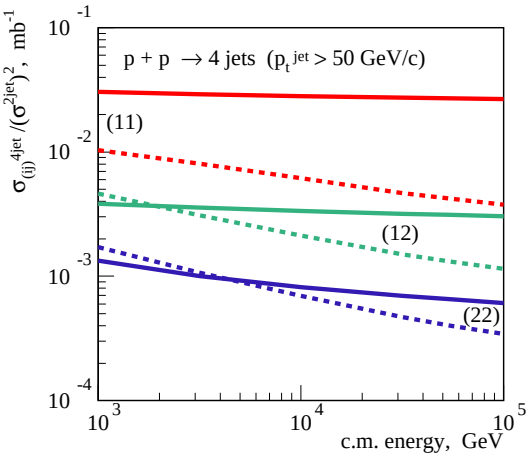

Figure **9**: Energy dependence of the ratios $2\sigma_{(ij)}^{4jet(2v2)}/\left(\sigma_{pp}^{2jet}\right)^2$ (solid lines) and $2\sigma_{(ij)}^{4jet(2v1)_h}/\left(\sigma_{pp}^{2jet}\right)^2$ (dashed lines) for DPS production of two dijets of $p_t^{jet} > 50$ GeV/c for different combinations of parton Fock states (ij), as indicated in the figure.

$2\sigma_{(ij)}^{4jet(2v2)}/\left(\sigma_{pp}^{2jet}\right)^2$ and $2\sigma_{(ij)}^{4jet(2v1)_h}/\left(\sigma_{pp}^{2jet}\right)^2$ for different combinations of the large- and small-size diffractive eigenstates as a function of $\sqrt{s}$. Thus, the quicker decrease of the ratio of the total $(2v1)_h$ to (2v2) contributions, $R_{(2v1)_h}$, in Fig. 8 is explained by the fact that with increasing energy the interactions involving small-size parton Fock states contribute less to the DPS cross sections $\sigma_{pp}^{4jet(\alpha)}(s, p_t^{cut})$ $[\alpha = (2v2), (2v1)_s, (2v1)_h]$, compared to the case when both interacting protons are represented by their largest size Fock states.

It is noteworthy that there is a number of other effects which contribute to the uncertainty of the hard parton splitting contribution and which have led to the much smaller values of $R_{(2v1)_h}$, obtained in this work, compared to previous calculations in Refs. [11, 23]. For example, our choice of the factorization scale, $M_F^2 = p_t^2/4$, shortens somewhat the kinematic range available for the perturbative parton evolution, compared to the standard choice ($M_F^2 = p_t^2$), which reduces the respective collinear enhancements. The corresponding uncertainty is related to higher-order effects of which the potential importance has already been stressed in Ref. [11]. Another effect is the sensitivity of $R_{(2v1)_h}$ to the chosen functional form for the two-gluon form factor. For example, replacing the dipole ansatz used in Ref. [11] by a Gaussian reduces $R_{(2v1)_h}$ by $\simeq 17\%$ [see Eqs. (19-21) in that reference]. Additionally, the relative importance of the perturbative parton splitting for DPS depends noticeably on both the large and small x behavior of gluon PDF, $G(x, Q_0^2)$. A steeper low-x rise of $G(x, Q_0^2)$ would enhance the (2v2) contribution, compared to $(2v1)_h$, and thus reduce $R_{(2v1)_h}$ (see Eq. (5) of Ref. [11]). On the other hand, a harder large-x shape of the gluon PDF would, on the contrary, enhance the hard splitting contribution, while leaving the (2v2) contribution practically unchanged.

Finally, we have to mention that the obtained values of σ_{pp}^{eff} are systematically higher than the measured values, though consistent with them within the reported experimental accuracies. Clearly, the above-discussed uncertainties concerning the contribution of the perturbative parton splitting give one enough freedom to adjust $R_{(2v1)_h}$ and thereby to approach experimental measurements. However, the nonperturbative effects studied in this work are also subject to substantial uncertainties related, e.g. to the strength of the triple-Pomeron coupling, which controls the magnitude of the soft parton splitting contribution. On the other hand, the employed Good-Walker–like scheme with only two diffractive eigenstates is rather crude, and a more advanced treatment is generally desirable. Hence, we may only speak here about a semiquantitative approach to the problem.

4 Conclusions

In this work, we applied the phenomenological Reggeon field theory framework to investigate the relative importance of perturbative and nonperturbative multiparton correlations for the treatment of double parton scattering in proton-proton collisions. We obtained a significant correction to the effective cross section for DPS due to nonperturbative parton splitting. When combined with the contribution of perturbative parton splitting, this results in a rather weak energy and transverse momentum dependence of $\sigma_{pp}^{\rm eff}$, in agreement with experimental observations. On the other hand, we observed that color fluctuations have a noticeable impact on the calculated rates of double parton scattering and on the relative role of the perturbative parton splitting mechanism.

While the obtained numerical results bear a substantial model dependence, the observed qualitative trends are of general character and can probably be reproduced applying other alternative approaches to the problem, for example, using the original color fluctuations framework of Ref. [37].

Acknowledgments

The authors acknowledge useful discussions with B. Blok and M. Strikman. This work was supported in part by Deutsche Forschungsgemeinschaft (Project No. OS 481/1-1) and the State of Hesse via the LOEWE-Center HIC for FAIR.

References

[1] CDF Collaboration, F. Abe *et al.*, Phys. Rev. Lett. **79**, 584 (1997); Phys. Rev. D **56**, 3811 (1997).

[2] D0 Collaboration, V. M. Abazov *et al.*, Phys. Rev. D **81**, 052012 (2010).

[3] ATLAS Collaboration, G. Aad *et al.*, New J. Phys. **15**, 033038 (2013).

[4] CMS Collaboration, S. Chatrchyan *et al.*, JHEP **03**, 032 (2014).

[5] N. Paver and D. Treleani, Nuovo Cim. A **70**, 215 (1982); Z. Phys. C **28**, 187 (1985).

[6] V. P. Shelest, A. M. Snigirev, and G. M. Zinovjev, Phys. Lett. B **113**, 325 (1982).

[7] M. Mekhfi, Phys. Rev. D **32**, 2371 (1985).

[8] T. Sjostrand and M. van Zijl, Phys. Rev. D **36**, 2019 (1987).

[9] B. Blok, Yu. Dokshitzer, L. Frankfurt, and M. Strikman, Phys. Rev. D **83**, 071501 (2011).

[10] B. Blok, Yu. Dokshitzer, L. Frankfurt, and M. Strikman, Eur. Phys. J. C **72**, 1963 (2012).

[11] B. Blok, Yu. Dokshitzer, L. Frankfurt, and M. Strikman, Eur. Phys. J. C **74**, 2926 (2014).

[12] M. G. Ryskin and A. M. Snigirev, Phys. Rev. D **83**, 114047 (2011).

[13] M. Diehl, D. Ostermeier, and A. Schafer, JHEP **1203**, 089 (2012).

[14] J. R. Gaunt, JHEP **1301**, 042 (2013).

[15] B. Blok, M. Strikman, and U. A. Wiedemann, Eur. Phys. J. C **73**, 2433 (2013).

[16] S. Salvini, D. Treleani and G. Calucci, Phys. Rev. D **89**, 016020 (2014).

[17] S. J. Brodsky, L. Frankfurt, J. F. Gunion, A. H. Mueller, and M. Strikman, Phys. Rev. D **50**, 3134 (1994).

[18] L. Frankfurt and M. Strikman, Phys. Rev. D **66**, 031502(R) (2002).

[19] H1 Collaboration, C. Adloff *et al.*, Phys. Lett. B **483**, 23 (2000).

[20] ZEUS Collaboration, S. Chekanov *et al.*, Eur. Phys. J. C **24**, 345 (2002).

[21] L. Frankfurt, M. Strikman and C. Weiss, Phys. Rev. D **69**, 114010 (2004).

[22] A. M. Snigirev, Phys. Rev. D **81**, 065014 (2010).

[23] J. R. Gaunt, R. Maciula and A. Szczurek, Phys. Rev. D **90**, 054017 (2014).

[24] B. Blok and P. Gunnellini, Eur. Phys. J. C **75**, 282 (2015).

[25] B. Blok, Yu. Dokshitzer, L. Frankfurt, and M. Strikman, arXiv:1206.5594 [hep-ph].

[26] V. N. Gribov, Sov. Phys. JETP **26**, 414 (1968).

[27] S. Ostapchenko, Phys. Rev. D **74**, 014026 (2006).

[28] S. Ostapchenko, Phys. Rev. D **83**, 014018 (2011).

[29] O. V. Kancheli, JETP Lett. **18**, 274 (1973); J. L. Cardi, Nucl. Phys. B **75**, 413 (1974).

[30] A. B. Kaidalov, L. A. Ponomarev and K. A. Ter-Martirosyan, Sov. J. Nucl. Phys. **44**, 468 (1986).

[31] S. Ostapchenko, Phys. Lett. B **636**, 40 (2006); Phys. Rev. D **77**, 034009 (2008).

[32] H.J. Drescher, M. Hladik, S. Ostapchenko, and K. Werner, J. Phys. G **25**, L91 (1999).

[33] H.J. Drescher, M. Hladik, S. Ostapchenko, T. Pierog, and K. Werner, Phys. Rep. **350**, 93 (2001).

[34] S. Ostapchenko, H.J. Drescher, F.M. Liu, T. Pierog, and K. Werner, J. Phys. G **28**, 2597 (2002).

[35] M. L. Good and W. D. Walker, Phys. Rev. **120**, 1857 (1960).

[36] A. B. Kaidalov, Phys. Rep. **50**, 157 (1979).

[37] L. Frankfurt, M. Strikman, D. Treleani and C. Weiss, Phys. Rev. Lett. **101**, 202003 (2008).

[38] S. Ostapchenko, arXiv:hep-ph/0501093.

[39] E. Gotsman, E. Levin, U. Maor and J. S. Miller, Eur Phys. J. C **57**, 689 (2008).

[40] D. Treleani, Phys. Rev. D **76**, 076006 (2007).